Electronic Supplementary Material (ESI) for Journal of Materials Chemistry A.


# Coupling Core-Shelled Bi@Void@$TiO_2$ Heterostructures into Carbon Nanofibers for Achieving Fast Potassium Storage and Long Cycling Stability

*Zongying Gao, Liang Han, Hui Gao, Jingwei Chen,* Zining Sun, Chunliu Zhu, Yafei Zhang, Jing Shi, Shougang Chen,* Huanlei Wang**

College of Materials Science and Engineering, Ocean University of China, Qingdao 266100, China

* Corresponding author. E-mail: chenjingwei@ouc.edu.cn; sgchen@ouc.edu.cn; huanleiwang@gmail.com

*Computational Methods:* We used the first principle calculation method based on density functional theory (DFT) to optimize the structure and calculate the properties of Bi, $TiO_2$ and Bi/$TiO_2$ heterostructures. The CASTEP software package of DFT was used to calculate the structure, using the generalized-gradient approximation perdew-burke-ernzerhof (GGA-PBE) exchange correlation functional, and the interaction between atoms was simulated by the super soft pseudopotential method. The CASTEP software package requires that the calculation system must be periodic, and the calculation requires that there should be a large enough vacuum layer in our structure to accurately judge the energy level at the vacuum and eliminate the influence of interlayer interaction, thereby a vacuum layer was added as needed. We constructed Bi, $TiO_2$ and Bi/$TiO_2$ heterojunction models, and added a vacuum layer in the Z direction. Broyden-fletcher-goldfarb-shanno (BFGS) optimization algorithm is used for geometric optimization. The atomic energy convergence criterion is $2.0 \times 10^{-6}$ eV, the convergence standard of atomic interaction force is 0.05 eV, the stress convergence standard is 0.1 GPa, and the convergence standard of atomic maximum displacement is $2.0 \times 10^{-3}$ Å, the truncation energy was set as 300 eV, and the k-point of brillouin zone generated by gamma method was set as $2\times2\times2$ to meet the geometric relationship of reciprocal space.

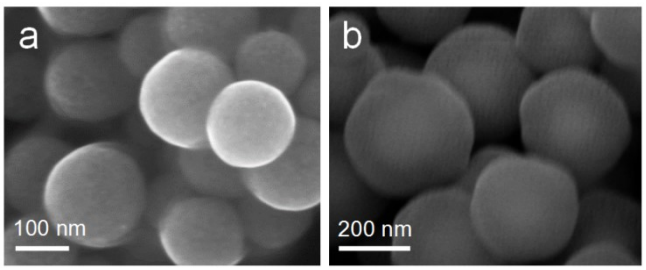


**Figure. S1.** SEM images of (a) Bi, and (b) Bi@$SiO_2$.

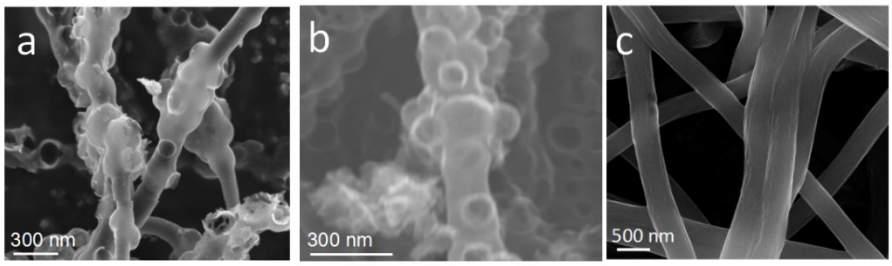


**Figure. S2.** SEM images of (a) Bi@Void⊂CNF, (b) Void@$TiO_2$⊂CNF, and (c) pure carbon.

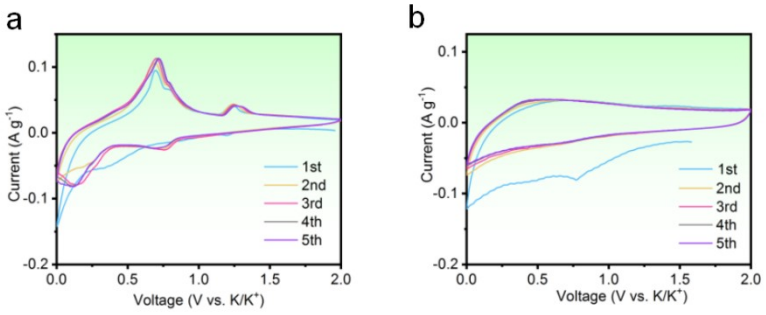


**Figure. S3.** CV curves of (a) Bi@Void⊂CNF, and (b) Void@$TiO_2$⊂CNF at the scan rate of 0.1 mV $s^{-1}$.

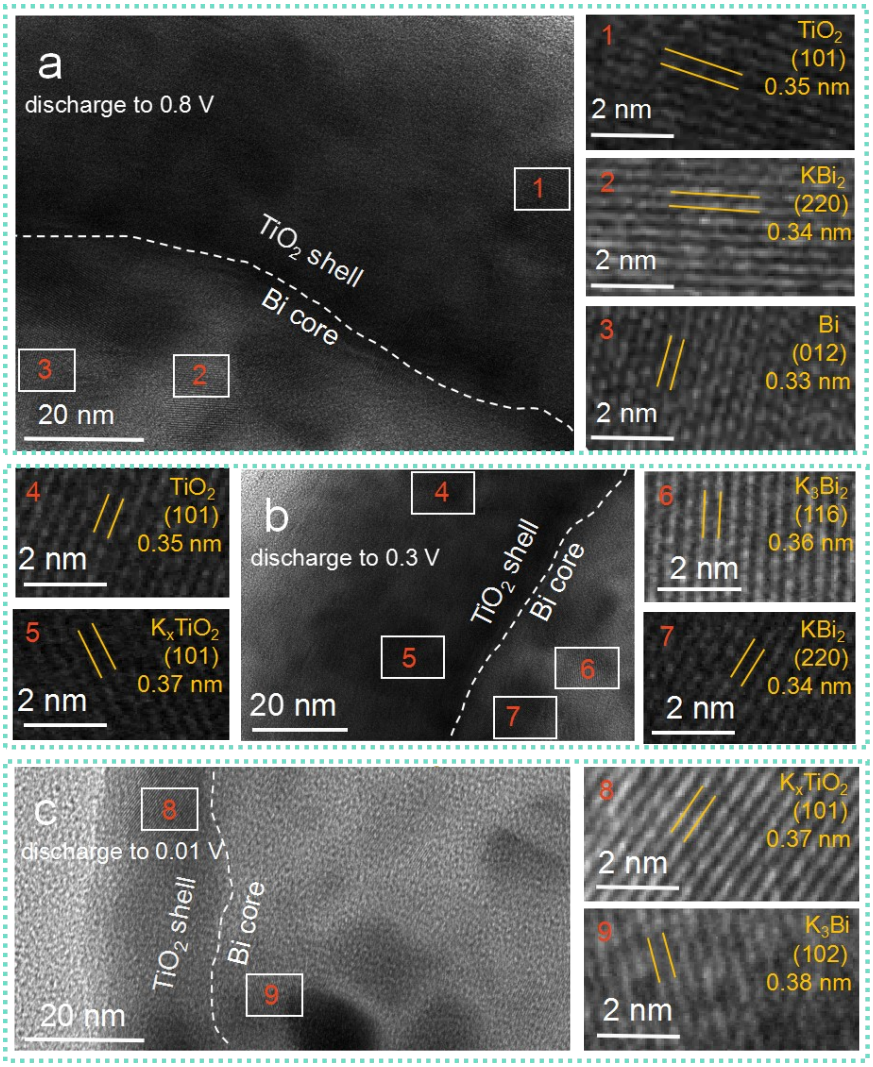


**Figure. S4.** Ex-situ high-resolution TEM images for Bi@Void@$TiO_2$⊂CNF anodes: a) after discharge to 0.8 V, b) after discharge to 0.3 V, and (c) after discharge to 0.01 V.

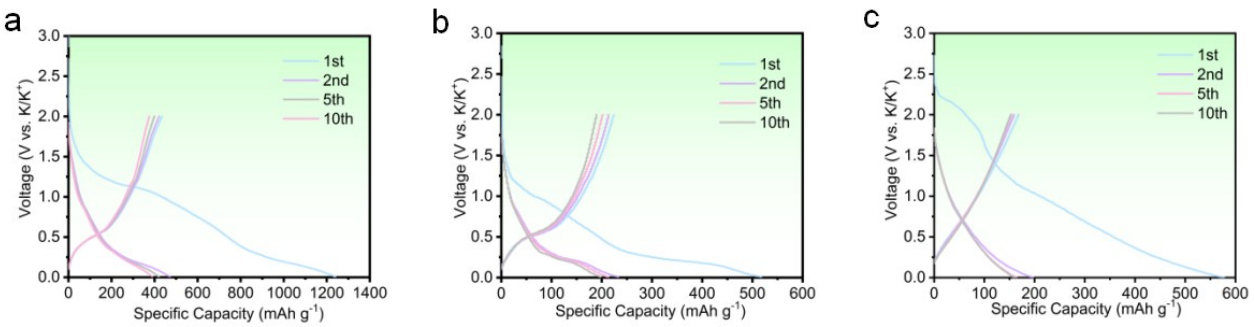


**Figure. S5.** Galvanostatic charge-discharge profiles at 0.05 A $g^{-1}$ of (a) Bi@Void@$TiO_2$⊂CNF, (b) Bi@Void⊂CNF, and (c) Void@$TiO_2$⊂CNF.

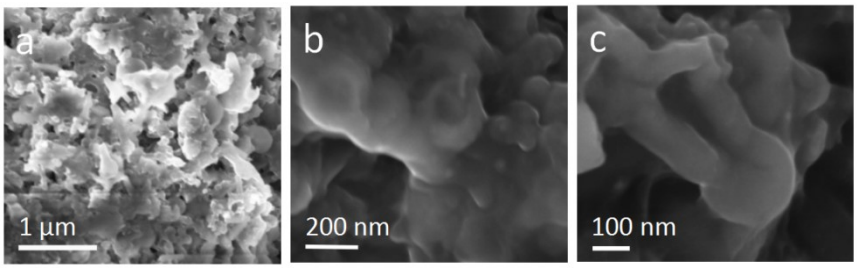


**Figure. S6.** SEM images of Bi@Void@$TiO_2$⊂CNF after 1000 cycles at 2 A $g^{-1}$.

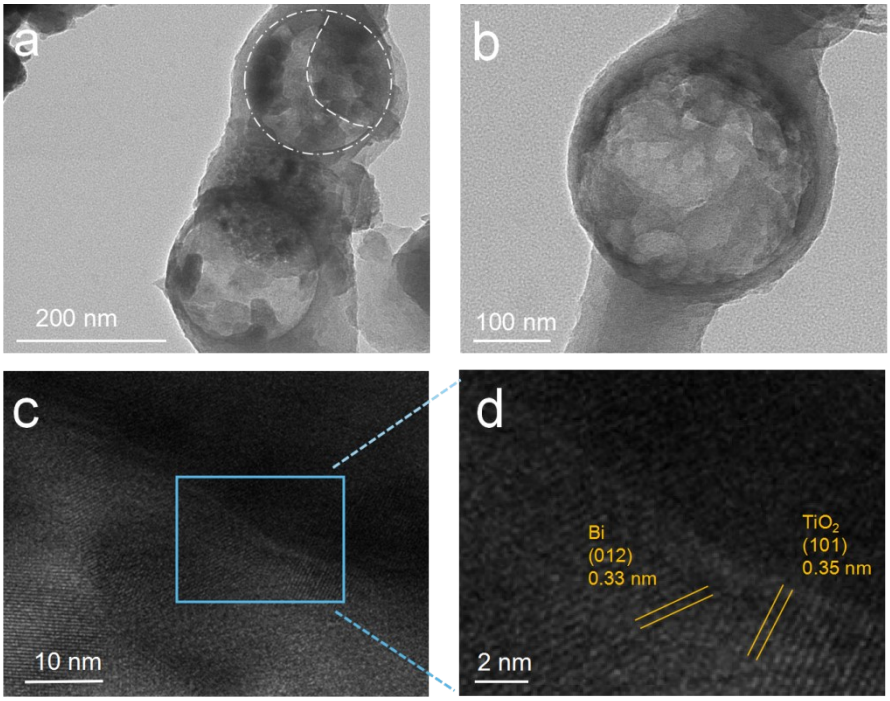


**Figure. S7.** TEM and high-resolution TEM images of Bi@Void@$TiO_2$⊂CNF after 1000 cycles at 2 A $g^{-1}$.

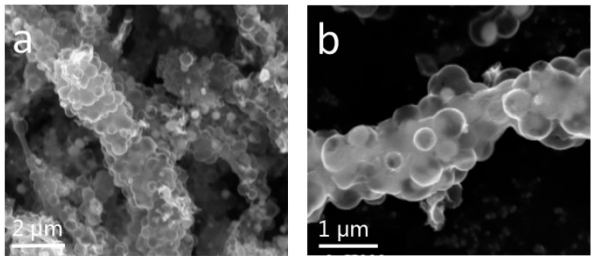


**Figure. S8.** a, b) SEM images of (Bi@Void@$TiO_2$)1.2⊂CNF.

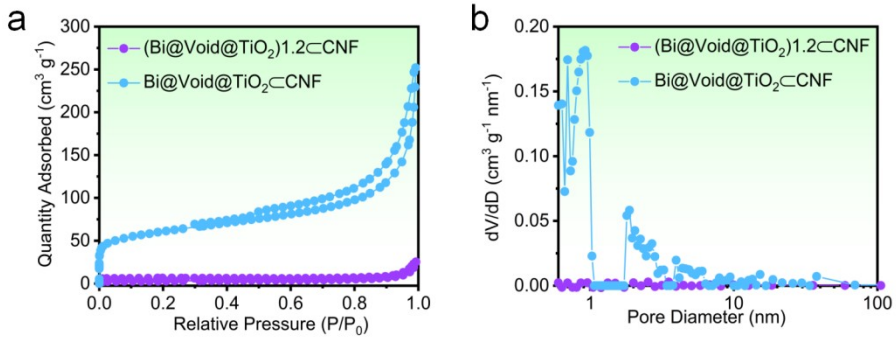


**Figure. S9.** a) Nitrogen adsorption-desorption isotherms, and (b) pore size distributions of (Bi@Void@$TiO_2$)1.2⊂CNF, and Bi@Void@$TiO_2$⊂CNF.

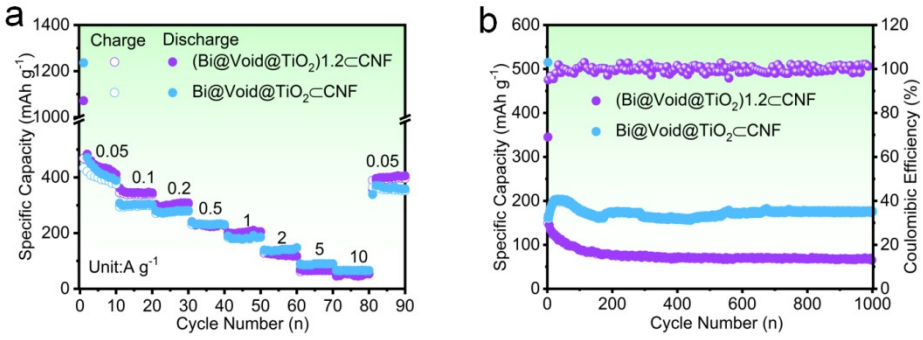


**Figure. S10.** a) Rate performance and (b) cycling performance of Bi@Void@$TiO_2$⊂CNF and (Bi@Void@$TiO_2$)1.2⊂CNF at 2 A $g^{-1}$.

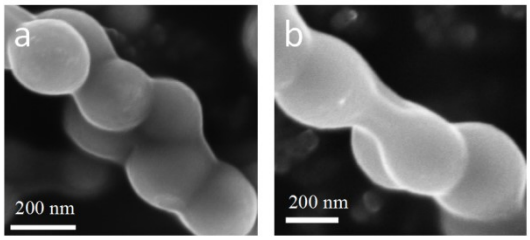


**Figure. S11.** SEM images of (a) Bi@Void@$TiO_2$(0.5)⊂CNF and (b) Bi@Void@$TiO_2$(1.5)⊂CNF.

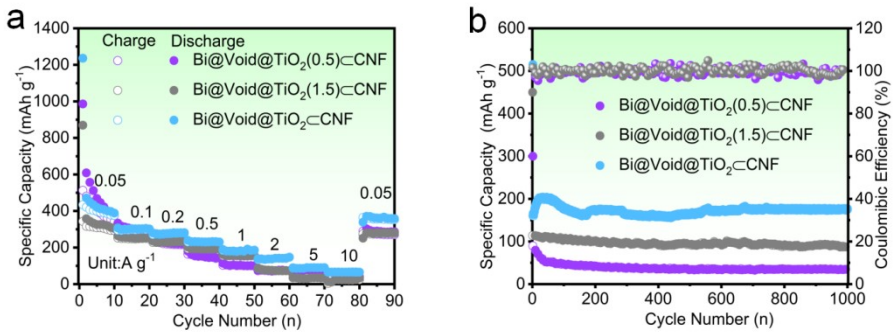


**Figure. S12.** Electrochemical performance of Bi@Void@$TiO_2$⊂CNF, Bi@Void@$TiO_2$(0.5)⊂CNF *and* Bi@Void@$TiO_2$(1.5)⊂CNF. a) Rate performance and (b) cycling performance at 2 A $g^{-1}$.

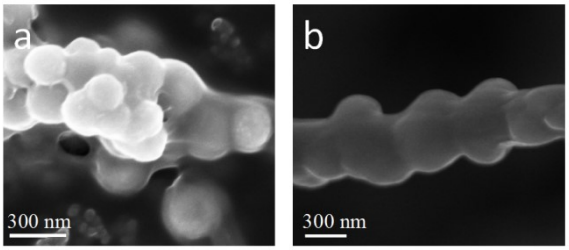


**Figure. S13.** SEM images of (a) Bi@Void(8)@$TiO_2$⊂CNF and (b) Bi@Void(12)@$TiO_2$⊂CNF.

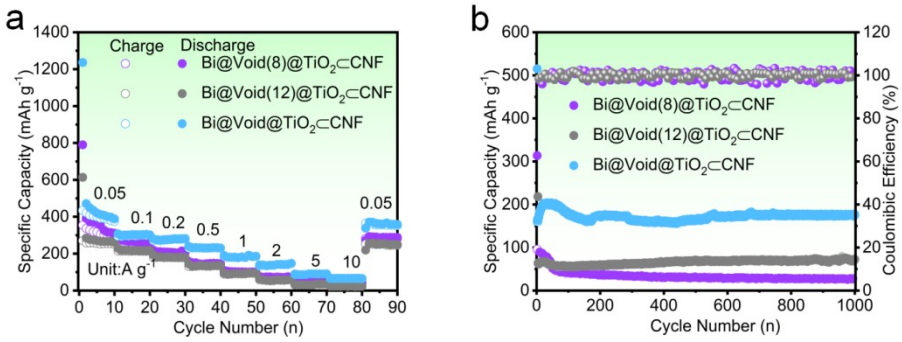


**Figure. S14.** Electrochemical performance of Bi@Void(8)@$TiO_2$⊂CNF, Bi@Void@$TiO_2$⊂CNF *and* Bi@Void(12)@$TiO_2$⊂CNF. a) Rate performance and (b) cycling performance at 2 A $g^{-1}$.

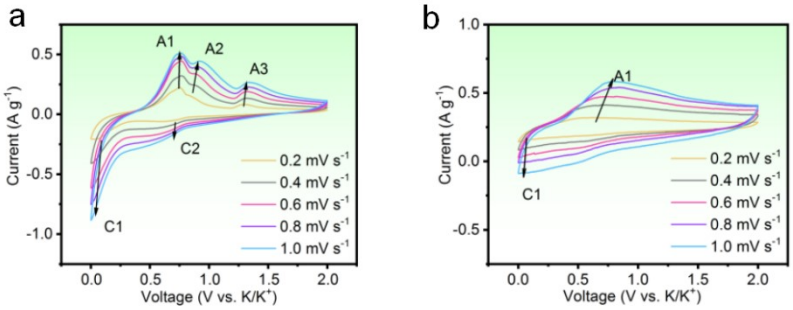


**Figure. S15.** CV curves of (a) Bi@Void⊂CNF, and (b) Void@$TiO_2$⊂CNF at the different scan rates.

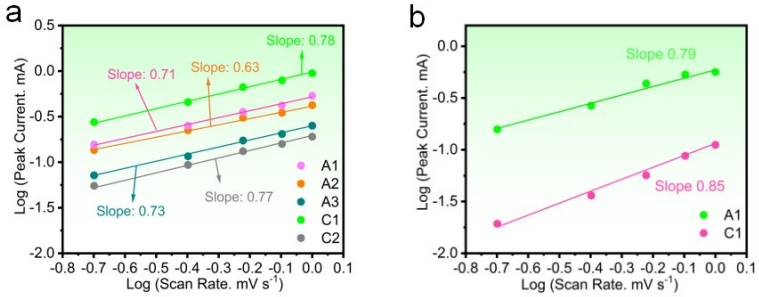


**Figure. S16.** *b* values of peak current: (a) Bi@Void⊂CNF, and (b) Void@$TiO_2$⊂CNF.

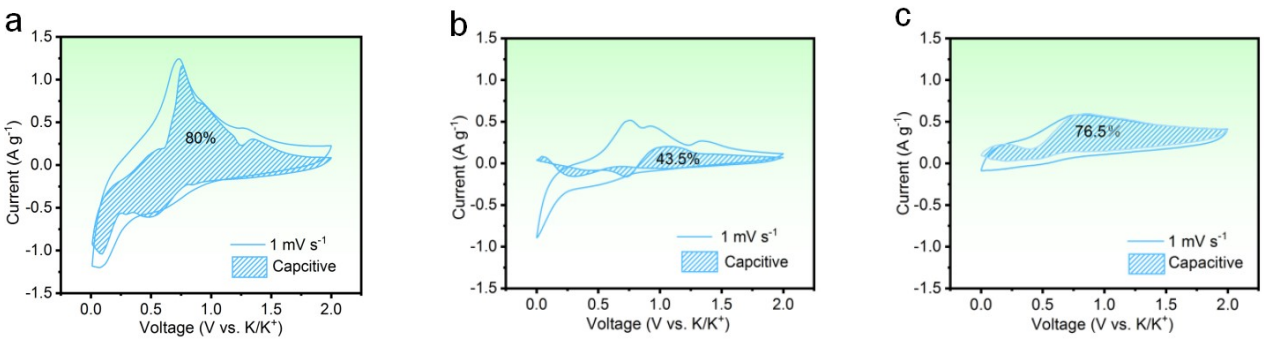


**Figure. S17.** Capacitive storage contribution (shade area) of (a) Bi@Void@$TiO_2$⊂CNF, (b) Bi@Void⊂CNF, and (c) Void@$TiO_2$⊂CNF at a scan rate of 1 mV $s^{-1}$.

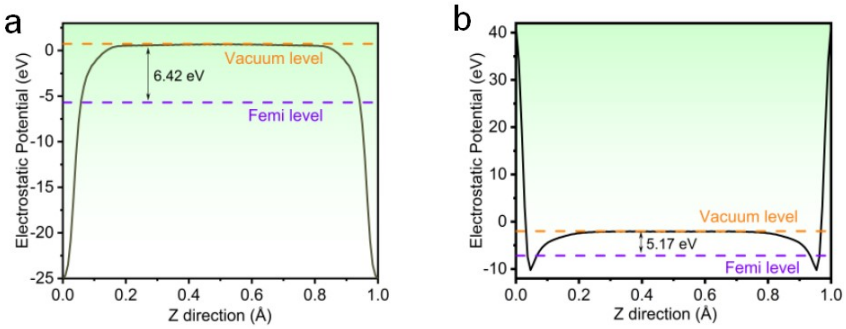


**Figure. S18.** Electrostatic potential drop diagram of (a) Bi homogeneous junction, and (b) $TiO_2$ homogeneous junction.

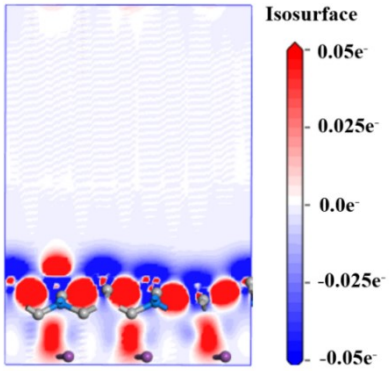


**Figure. S19.** Side view of an interlayer differential charge density diagram for a Bi/$TiO_2$ heterostructure.

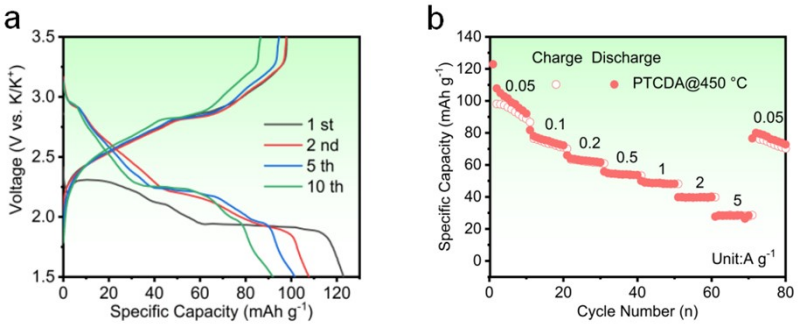


**Figure. S20.** a) Galvanostatic charge-discharge profiles at 0.05 A $g^{-1}$, and (b) rate cycling behavior of PTCDA@450 °C.

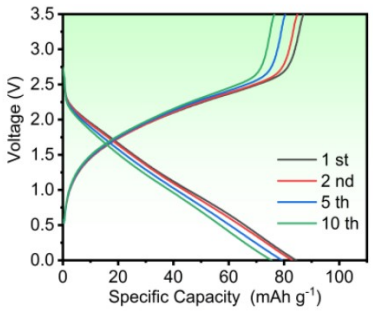


**Figure. S21.** Galvanostatic charge-discharge profiles at 0.2 A $g^{-1}$ of Bi@Void@$TiO_2$⊂CNF based K-ion full cell.

**Table. S1.** Physical and electrochemical properties of Bi@Void@$TiO_2$⊂CNF, Bi@Void⊂CNF and Void@$TiO_2$⊂CNF samples.

| Sample | $S_{BET}$[a] ($m^2\ g^{-1}$) | $V_t$[b] ($cm^3\ g^{-1}$) | Pore vol (%) | |
|---|---|---|---|---|
| | | | $V_{0\text{-}2\ nm}$ | $V_{>2\ nm}$ |
| Bi@Void@$TiO_2$⊂CNF | 215.53 | 0.46 | 24.96 | 75.04 |
| Bi@Void⊂CNF | 18.76 | 0.08 | 0.16 | 99.84 |
| Void@$TiO_2$⊂CNF | 171.69 | 0.58 | 0 | 100 |

[a] Specific surface area was calculated by the Brunauer-Emmett-Teller (BET) method.
[b] Total pore volume was determined by the density functional theory (DFT) method.

**Table. S2.** Electrochemical performance of alloy-based anodes for PIBs.

| Anode | Current density ($A\ g^{-1}$) | Cycle Number (n) | Capacity ($mAh\ g^{-1}$) | Rate ($mAh\ g^{-1}$/ $A\ g^{-1}$) | References |
|---|---|---|---|---|---|
| G-$TiO_2$ NTs | 0.5 | 2000 | 160 | 129/5 | 1 |
| HeTi$O_2$eC MTs | 0.5 | 1200 | 133 | 97/2 | 2 |
| $TiO_2$/C | 0.05 | 1000 | 259 | 150/1 | 3 |
| $TiO_2$/RGO | 1 | 1000 | 85 | 107/1 | 4 |
| Bi/rGO | 0.05 | 200 | 100 | 235/0.5 | 5 |
| Bi@3DGFs | 1 | 400 | 164 | 113/5 | 6 |
| BiND/G | 5 | 500 | 213 | 200/10 | 7 |
| Bi@C-1000 | 0.5 | 300 | 179 | 186/1.5 | 8 |
| BiSb@C | 0.5 | 600 | 320 | 152/2 | 9 |
| Sb@CNFs | 1 | 1000 | 227 | 121/2 | 10 |
| SnSb@NC | 0.5 | 200 | 185 | 116/2 | 11 |
| Sb/CNS | 0.2 | 600 | 247 | 101/2 | 12 |
| $Sb_{0.5}Bi_{0.5}$@C | 0.5 | 400 | 226 | 190/2 | 13 |
| Sn/NPC | 0.05 | 200 | 198 | 22/2 | 14 |
| **This work** | **2** | **3000** | **171** | **65/10** | **-** |

**References**


1 J. Cai, R. Cai, Z. Sun, X. Wang, N. Wei, F. Xu, Y. Shao, P. Gao, S. Dou and J. Sun, *Nano-Micro Lett.*, 2020, **12**, 123.

2 Y. Li, C. Yang, F. Zheng, Q. Pan, Y. Liu, G. Wang, T. Liu, J. Hu and M. Liu, *Nano Energy*, 2019, **59**, 582–590.

3 D. Su, Y. Pei, L. Liu, Z. Liu, J. Liu, M. Yang, J. Wen, J. Dai, H. Deng and G. Cao, *Nano-Micro Lett.*, 2021, **13**, 107.

4 Y. Fang, R. Hu, B. Liu, Y. Zhang, K. Zhu, J. Yan, K. Ye, K. Cheng, G. Wang and D. Cao, *J. Mater. Chem. A*, 2019, **7**, 5363–5372.

5 Q. Zhang, J. Mao, W. K. Pang, T. Zheng, V. Sencadas, Y. Chen, Y. Liu and Z. Guo, *Adv. Energy Mater.*, 2018, **8**, 1703288.

6 X. Cheng, D. Li, Y. Wu, R. Xu and Y. Yu, *J. Mater. Chem. A*, 2019, **7**, 4913–4921.

7 Y. Zhao, X. Ren, Z. Xing, D. Zhu, W. Tian, C. Guan, Y. Yang, W. Qin, J. Wang, L. Zhang, Y. Huang, W. Wen, X. Li and R. Tai, *Small*, 2020, **16**, 1905789.

8 X. Xiang, D. Liu, X. Zhu, K. Fang, K. Zhou, H. Tang, Z. Xie, J. Li, H. Zheng and D. Qu, *Appl. Surf. Sci.*, 2020, **514**, 145947.

9 P. Xiong, J. Wu, M. Zhou and Y. Xu, *ACS Nano*, 2020, **14**, 1018–1026.

10 H. Huang, J. Wang, X. Yang, R. Hu, J. Liu, L. Zhang and M. Zhu, *Angew. Chem. Int. Ed.*, 2020, **132**, 14612–14618.

11 Z. Wang, K. Dong, D. Wang, S. Luo, Y. Liu, Q. Wang, Y. Zhang, A. Hao, C. Shi and N. Zhao, *J. Mater. Chem. A*, 2019, **7**, 14309–14318.

12 Y. Han, T. Li, Y. Li, J. Tian, Z. Yi, N. Lin and Y. Qian, *Energy Storage Mater.*, 2019, **20**, 46–54.

13 X.-D. He, J.-Y. Liao, S. Wang, J.-R. Wang, Z.-H. Liu, X. Ding, Q. Hu, Z.-Y. Wen and C.-H. Chen, *J. Mater. Chem. A*, 2019, **7**, 27041–27047.

14 Y. Yang, D. Li, J. Zhang, G. Suo, Q. Yu, L. Feng, X. Hou, X. Ye, L. Zhang and W. Wang, *Mater. Lett.*, 2019, **256**, 126613.